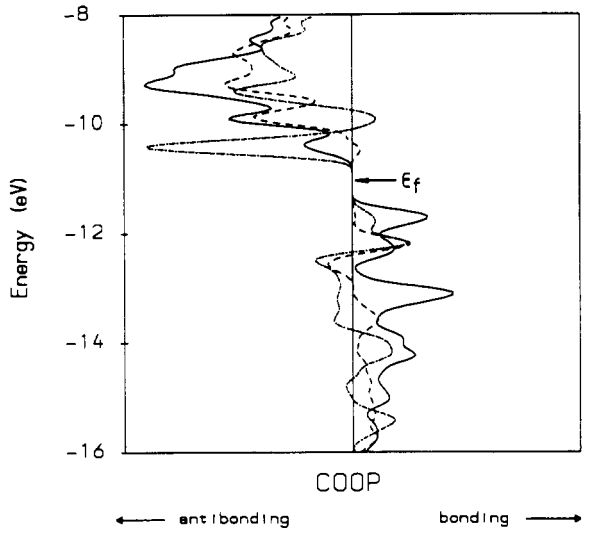

Figure 5. Crystal orbital overlap population (COOP) curves for Nb_2Te_6I: solid line, Nb(2)-Nb(2A); dashed line, Nb(1)-Nb(2); dashed-dotted line, Nb(1)-Nb(2A).

and the Nb(1)-Nb(2) contributions. The most remarkable feature is that, for this particular electron count, bonding interactions are maximized. Below the band gap, strongly metal-metal-bonding states are being filled; above the gap, the corresponding antibonding states remain empty. Figure 4 shows clearly that the metal-metal bond lengths parallel the (computed) bond strengths, i.e., the Nb(2)-Nb(2A) bond is significantly stronger than the other ones.

The COOP curve also supports the result of the crystal structure analysis. It is a well-known fact that the distinction between Te and I in X-ray work it not a trivial task. We were hesitant to assign Te(6) as tellurium rather than iodine. Choosing iodine, however, would have meant an electron count higher than d^1 on the metal atoms and filling strongly metal-metal-antibonding states as can be seen from Figure 5. Our final choice was determined from the analytical and computational results. Thus, Nb_2Te_6I may serve nicely to illustrate how semiempirical theoretical methods can prove extremely useful in crystal structure determination.

Acknowledgment. This work was supported by a grant from the Bundesministerium für Forschung und Technologie (BMFT) under Contract No. 05 439GXB 3. I am grateful to Prof. B. Krebs for additional support. The computing equipment was purchased through a grant from the Deutsche Forschungsgemeinschaft (DFG, Kr 406/9-1).

Supplementary Material Available: Table SI, listing full experimental details concerning the crystal structure determination, and Tables SII and SIII, listing thermal parameters and distances and angles (3 pages); a table of calculated and observed structure factors (15 pages). Ordering information is given on any current masthead page.

Contribution from the Department of Inorganic Chemistry, Indian Association for the Cultivation of Science, Calcutta 700 032, India

Two Manganese(IV) Complexes with Isomeric MnN_4O_2 Spheres Incorporating Hexadentate Amide-Amine-Phenolate Coordination

Swapan Kumar Chandra and Animesh Chakravorty*

Received July 24, 1991

The hexadentate ligands 1,8-bis(2-hydroxybenzamido)-3,6-diazaoctane (H_4L^2) and 1,10-bis(2-hydroxybenzamido)-4,7-diazadecane (H_4L^3) have been synthesized. These react with $Mn(CH_3CO_2)_3 \cdot 2H_2O$ in aqueous methanol in air affording crystalline $Mn^{IV}L^2 \cdot 4H_2O$ and $Mn^{IV}L^3 \cdot MeOH$ in excellent yields. Both complexes have the MnN_4O_2 coordination sphere. The amide nitrogen pairs are coordinated trans to each other in $Mn^{IV}L^2 \cdot 4H_2O$, whereas the phenolic oxygens are trans in $Mn^{IV}L^3 \cdot MeOH$. The coordinated amide groups are planar in both complexes. The Mn-N(amide), Mn-N(amine), and Mn-O(phenol) distances are respectively 1.953 (3), 1.954 (3); 2.034 (3), 2.041 (3); and 1.839 (2), 1.858 (3) Å in $MnL^2 \cdot 4H_2O$ and 1.922 (3), 1.945 (3); 2.073 (4), 2.095 (3); and 1.858 (3) Å in $MnL^3 \cdot MeOH$. Solvent oxygen, amide oxygen, and amine nitrogen atoms are involved in hydrogen bonding. Crystal data for $MnL^2 \cdot 4H_2O$ are as follows: chemical formula, $C_{20}H_{30}N_4O_8Mn$; crystal system, monoclinic; space group, $P2_1/n$; $a = 8.778$ (3), $b = 21.559$ (8), $c = 11.882$ (3) Å; $\beta = 99.40$ (2)°; $V = 2218$ (1) Å^3; $Z = 4$; $R = 4.57\%$, $R_w = 4.54\%$. Crystal data for $MnL^3 \cdot MeOH$ are as follows: chemical formula, $C_{23}H_{30}N_4O_5Mn$; crystal system, monoclinic; space group, $P2_1/n$; $a = 10.369$ (4), $b = 13.639$ (8), $c = 15.753$ (7) Å; $\beta = 95.61$ (3)°; $V = 2217$ (2) Å^3; $Z = 4$; $R = 4.58\%$, $R_w = 4.69\%$. The complexes have magnetic moments corresponding to the $3d^3$ configuration, and their X-band EPR spectra consist of weak and strong resonances at $g \sim 4$ and $g \sim 2$, respectively. In frozen methanol-toluene solution the latter resonance shows ^{55}Mn hyperfine structure and forbidden lines are also resolved. The axial zero field splitting parameter D (~ 0.012 cm^{-1}) is small compared to the X-band quantum. The amide-amine-phenolate ligand combination provides an effective electronic environment for the metal that is only slightly distorted in the ground state. In methanol solution quasireversible manganese(IV)-manganese(III) couples are observed with $E_{1/2}$ values of 0.01 and -0.07 V vs SCE in $MnL^2 \cdot 4H_2O$ and $MnL^3 \cdot MeOH$, respectively. The manganese(III) congeners can be electrogenerated in solution but are rapidly oxidized by air to the parent manganese(IV) species. The low metal reduction potentials are in line with the high pK values of the amide and aliphatic amine functions. These functions may not be important in photosystem II manganese binding.

Introduction

This work forms a part of our program on the synthesis, structure, and redox behavior of new mononuclear manganese(IV) complexes.[1-3] In the coordination environment of nonporphyrinic N,O donors such species are of interest in the biomimetic chemistry of the water oxidation site of photosystem II.[2-13] So far only a

(1) Pal, S.; Ghosh, P.; Chakravorty, A. *Inorg. Chem.* **1985**, *24*, 3704-3706.
(2) Chandra, S. K.; Basu, P.; Ray, D.; Pal, S.; Chakravorty, A. *Inorg. Chem.* **1990**, *29*, 2423-2428.
(3) Dutta, S.; Basu, P.; Chakravorty, A. *Inorg. Chem.* **1991**, *30*, 4031-4037.
(4) Pavacik, P. S.; Huffman, J. C.; Christou, G. *J. Chem. Soc., Chem. Commun.* **1986**, 43-44.
(5) (a) Kessissoglou, D. P.; Li, X.; Butler, W. M.; Pecoraro, V. L. *Inorg. Chem.* **1987**, *26*, 2487-2492. (b) Saadeh, S. M.; Lah, M. S.; Pecoraro, V. L. *Inorg. Chem.* **1991**, *30*, 8-15. (c) Li, X.; Lah, M. S.; Pecoraro, V. L. *Acta Crystallogr.* **1989**, *C45*, 1517-1519.
(6) Chan, M. K.; Armstrong, W. H. *Inorg. Chem.* **1989**, *28*, 3777-3779.

0020-1669/92/1331-0760$03.00/0

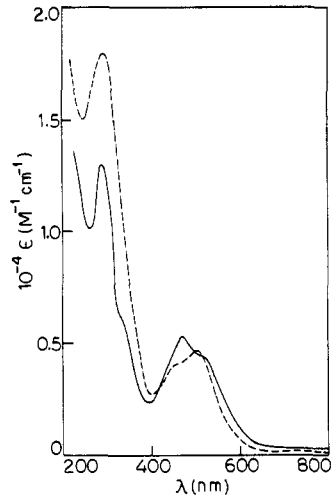

Figure 1. Electronic spectra of $MnL^2 \cdot 4H_2O$ (—) and $MnL^3 \cdot MeOH$ (---) in methanol.

small number of structurally authenticated complexes of this category have been described having coordination spheres MnN_6,[6] MnO_6,[5b,7] and MnN_2O_4.[2-5a,c]

In the present work a pair of hexadentate ligands incorporating amide, amine, and phenol functions have been designed and successfully employed for binding manganese(IV).[14] Both the complexes have been structurally characterized revealing the hitherto unreported nonporphyrinic $Mn^{IV}N_4O_2$ coordination sphere in two different geometrical forms.[15] We also have here the first structural authentication of the binding of manganese(IV) by amide and acyclic amine functions.[16] The EPR spectra of the complexes correspond to the relatively rare small axial distortion situation. The metal reduction potentials are low and spontaneous oxidation of $Mn^{III}N_4O_2$ to $Mn^{IV}N_4O_2$ occurs in air.

Results and Discussion

Synthesis. The two bis(2-hydroxybenzamido)diazaalkane ligands used in the present work are of type **1**, and these will be abbreviated as H_4L^x, where the four dissociable protons correspond

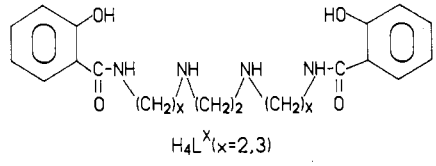

H_4L^x (x=2,3)

to the phenolic and amide functions. The value of x was varied with the purpose of observing the possible effect of methylene chain flexibility on coordination geometry. A stereochemical effect is

Table I. Electronic Spectral and Electrochemical[a] Data in Methanol at 298 K

complex	UV–vis data: λ_{max}, nm (ϵ, M^{-1} cm^{-1})	Mn(IV)–Mn(III) $E_{1/2}$, V (ΔE_p, mV)[c]	n[d]
$MnL^2 \cdot 4H_2O$	525[b] (4330), 465 (5325), 335[b] (6160), 285 (12900)	0.01 (100)	0.99
$MnL^3 \cdot MeOH$	505 (4714), 445[b] (3960), 290 (18023)	−0.07 (100)	0.98

[a] Supporting electrolyte is TEAP (0.1 M); working electrode is platinum; reference electrode is SCE. [b] Shoulder. [c] $E_{1/2}$ is calculated as the average of anodic (E_{pa}) and cathodic (E_{pc}) peak potentials; $\Delta E_p = E_{pa} - E_{pc}$. [d] Constant-potential coulometric (at −0.30 V) data with $n = Q/Q'$, where Q is the observed coulomb count and Q' is the calculated coulomb count for 1e transfer.

Table II. Selected Bond Distances (Å) and Angles (deg) and Their Estimated Standard Deviations for $MnL^2 \cdot 4H_2O$ and $MnL^3 \cdot MeOH$

$MnL^2 \cdot 4H_2O$		$MnL^3 \cdot MeOH$	
	Distances		
Mn–O(1)	1.839 (2)	Mn–O(1)	1.858 (3)
Mn–O(4)	1.858 (3)	Mn–O(4)	1.858 (3)
Mn–N(1)	1.953 (3)	Mn–N(1)	1.945 (3)
Mn–N(2)	2.034 (3)	Mn–N(2)	2.095 (3)
Mn–N(3)	2.041 (3)	Mn–N(3)	2.073 (4)
Mn–N(4)	1.954 (3)	Mn–N(4)	1.922 (3)
O(1)–C(1)	1.343 (4)	O(1)–C(1)	1.339 (5)
O(2)–C(7)	1.260 (4)	O(2)–C(7)	1.244 (5)
O(3)–C(14)	1.256 (4)	O(3)–C(16)	1.250 (5)
O(4)–C(20)	1.348 (4)	O(4)–C(22)	1.324 (4)
N(1)–C(7)	1.335 (4)	O(5)–C(23)	1.381 (7)
N(4)–C(14)	1.340 (4)	N(1)–C(7)	1.334 (5)
		N(4)–C(16)	1.341 (5)
	Angles		
O(1)–Mn–O(4)	93.2 (1)	O(1)–Mn–O(4)	171.6 (1)
O(1)–Mn–N(1)	91.6 (1)	O(1)–Mn–N(1)	91.4 (1)
O(1)–Mn–N(2)	171.3 (1)	O(1)–Mn–N(2)	89.2 (1)
O(1)–Mn–N(3)	92.5 (1)	O(1)–Mn–N(3)	83.9 (1)
O(1)–Mn–N(4)	91.4 (1)	O(1)–Mn–N(4)	94.4 (1)
O(4)–Mn–N(1)	95.8 (1)	O(4)–Mn–N(1)	95.6 (1)
O(4)–Mn–N(2)	91.5 (1)	O(4)–Mn–N(2)	86.5 (1)
O(4)–Mn–N(3)	168.1 (1)	O(4)–Mn–N(3)	88.4 (1)
O(4)–Mn–N(4)	90.7 (1)	O(4)–Mn–N(4)	89.1 (1)
N(1)–Mn–N(2)	80.7 (1)	N(1)–Mn–N(2)	87.4 (1)
N(1)–Mn–N(3)	94.5 (1)	N(1)–Mn–N(3)	169.6 (1)
N(1)–Mn–N(4)	172.7 (1)	N(1)–Mn–N(4)	98.5 (1)
N(2)–Mn–N(3)	84.2 (1)	N(2)–Mn–N(3)	83.2 (1)
N(2)–Mn–N(4)	95.8 (1)	N(2)–Mn–N(4)	173.0 (1)
N(3)–Mn–N(4)	78.7 (1)	N(3)–Mn–N(4)	91.2 (1)

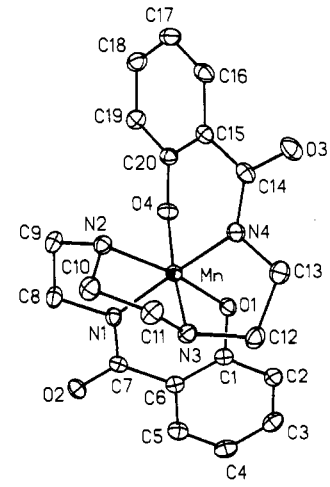

Figure 2. ORTEP plot and labeling scheme for MnL^2. All atoms are represented by their 30% probability ellipsoids.

(7) Hartman, J. R.; Foxman, B. M.; Cooper, S. R. *Inorg. Chem.* **1984**, *23*, 1381–1387.
(8) Kirby, J. A.; Robertson, A. S.; Smith, J. P.; Thompson, A. C.; Cooper, S. R.; Klein, M. P. *J. Am. Chem. Soc.* **1981**, *103*, 5529–5537.
(9) (a) Guiles, R. D.; Zimmermann, J. L.; McDermott, A. E.; Yachandra, V. K.; Cole, J. L.; Dexheimer, S. L.; Britt, R. D.; Wieghardt, K.; Bossek, U.; Sauer, K.; Klein, M. P. *Biochemistry* **1990**, *29*, 471–485. (b) Yachandra, V. K.; Guiles, R. D.; McDermott, A. E.; Britt, R. D.; Dexheimer, S. L.; Sauer, K.; Klein, M. P. *Biochim. Biophys. Acta* **1986**, *850*, 324–332.
(10) Tamura, N.; Ikeuchi, M.; Inoue, Y. *Biochim. Biophys. Acta* **1989**, *973*, 281–289.
(11) George, G. N.; Prince, R. C.; Cramer, S. P. *Science* **1989**, *243*, 789–791.
(12) Hansoon, O.; Aasa, R.; Vanngard, T. *Biophys. J.* **1987**, *51*, 825–832.
(13) Vincent, J. B.; Christou, G. *Adv. Inorg. Chem.* **1989**, *33*, 197–257.
(14) Preliminary communication reporting an incompletely refined structure of one complex: Chandra, S. K.; Choudhury, S. B.; Ray, D.; Chakravorty, A. *J. Chem. Soc., Chem. Commun.* **1990**, 474–475.
(15) Among porphyrins the $Mn^{IV}N_4O_2$ coordination sphere has been characterized in one case: Camenzind, M. J.; Hollander, F. J.; Hill, C. L. *Inorg. Chem.* **1982**, *21*, 4301–4308.
(16) Amide binding of manganese(IV) has been implicated in one system but without structural characterization: Koikawa, M.; Okawa, H.; Kida, S. *J. Chem. Soc., Dalton Trans.* **1988**, 641–645. Binding of an aromatic amine, viz., 2,2′-bipyridine is known.[4]

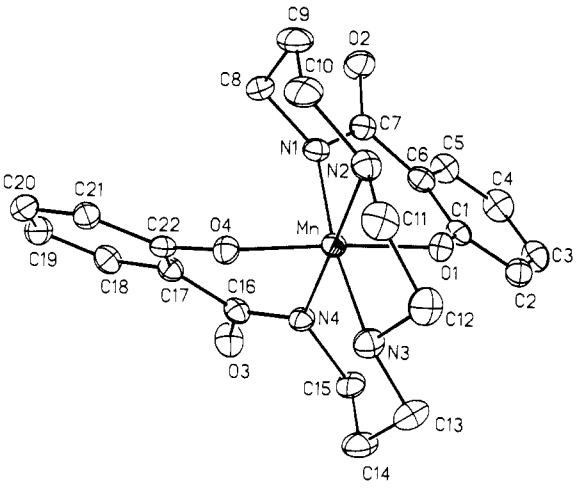

Figure 3. ORTEP plot and labeling scheme for MnL^3. All atoms are represented by their 30% probability ellipsoids.

indeed present; vide infra. The ligands are synthesized by mildly heating methyl or ethyl salicylate with amines taken in 2:1 mole ratio without the addition of any solvent.

The dark colored complexes are prepared in excellent yields by reacting the ligands with manganese(III) acetate dihydrate in 1:1 mole ratio in aqueous methanol in air, which acts as the oxidant. The chelates crystallize in characteristically different solvated forms from the same solvent (aqueous methanol) and are isolated as such: $MnL^2{\cdot}4H_2O$ and $MnL^3{\cdot}MeOH$. All solution measurements reported in this work were made in methanol.

The complexes absorb strongly in the visible and near-UV regions (Table I). A band and a shoulder are observed around 500 nm in both cases, but their relative positions differ in a characteristic manner (Figure 1). A band system in the same region has been observed in other families[2,3,5a] of mononuclear manganese(IV) complexes involving phenolato coordination. A probable origin is phenolate → manganese(IV) charge transfer.

Crystal and Molecular Structures. Atom-labeling schemes and molecular views of $MnL^2{\cdot}4H_2O$ and $MnL^3{\cdot}MeOH$ are shown (without solvent molecules) in Figures 2 and 3. Selected bond distances and angles are listed in Table II. In both cases the metal is bonded in the hexadentate distorted octahedral MnN_4O_2 fashion. To our knowledge the present complexes represent the only known structurally characterized manganese(IV) amide species; further no monomanganese(IV) complex incorporating an acyclic amine function appears to have been reported.[16]

A fundamental geometric difference between the two structures lies in the isomeric nature of coordination spheres. The amide nitrogen pairs are coordinated trans to each other in $Mn^{IV}L^2{\cdot}4H_2O$, whereas the phenolic oxygens are trans in $Mn^{IV}L^3{\cdot}MeOH$. The two coordinating ONN ligand halves are meridional in $MnL^2{\cdot}4H_2O$ but are facial in $MnL^3{\cdot}MeOH$. The difference is sustained by the greater flexibility of the trimethylene chains compared to the dimethylene chains. Of the five chelate rings two are six-membered and three are five-membered in $MnL^2{\cdot}4H_2O$. The corresponding numbers in $MnL^3{\cdot}MeOH$ are four and one, respectively. The dimethylene bridges have the gauche configuration, and the six-membered trimethylene containing rings in $MnL^3{\cdot}MeOH$ have chairlike configurations.

The coordinated amide groups in $MnL^2{\cdot}4H_2O$ are planar within experimental error. The mean deviations from the best Mn–N(1)–C(7)–O(2)–C(8) and Mn–N(4)–C(13)–O(3)–C(14) planes are respectively 0.03 and 0.01 Å. In $MnL^3{\cdot}MeOH$ planarity is less exact, mean deviations being 0.07 Å for the Mn–N(1)–C(7)–O(2)–C(8) plane and 0.08 Å for the Mn–N(4)–C(15)–O(3)–C(16) plane. Instances of large deviation from planarity in bonded amide functions have been documented in complexes of highly oxidized metal ions.[17,18]

(17) Collins, T. J.; Coots, R. J.; Furutani, T. T.; Keech, J. T.; Peake, G. T.; Santarsiero, B. D. *J. Am. Chem. Soc.* **1986**, *108*, 5333–5339.

Table III. Magnetic Moments and EPR Data

compd	μ_{eff},[a] μ_B	*g* values	*A*, G	*D*, G
$MnL^2{\cdot}4H_2O$	4.05	2.02,[b] 3.79;[b] 2.02,[c] 3.83;[c] 2.00,[d] 4.20[d]	97 ± 1[d]	125 ± 10[d]
$MnL^3{\cdot}MeOH$	4.03	2.02,[b] 4.34;[b] 2.02,[c] 4.30;[c] 2.02,[d] 4.09[d]	97 ± 1[d]	128 ± 8[d]

[a] In the solid state at 298 K. [b] Powder at 300 K. [c] Powder at 77 K. [d] Methanol–toluene (1:1) glass at 77 K.

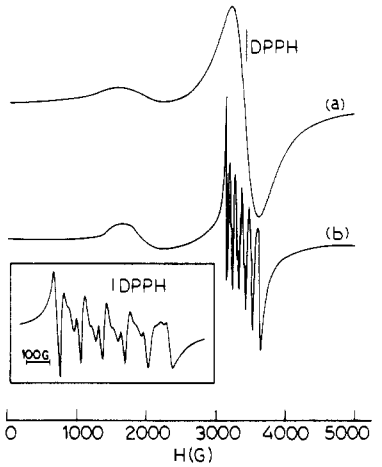

Figure 4. X-band EPR spectra at 77 K: (a) $MnL^3{\cdot}MeOH$ in polycrystalline form; (b) $MnL^3{\cdot}MeOH$ in methanol–toluene (1:1). The inset shows a pair of relatively weak "forbidden" transitions of the six hyperfine lines.

Bond distances in $MnL^2{\cdot}4H_2O$ and $MnL^3{\cdot}MeOH$ are quite alike (Table II). The Mn–N(amide) lengths are 1.953 (3), 1.954 (3) Å in $MnL^2{\cdot}4H_2O$ and 1.922 (3), 1.945 (3) Å in $MnL^3{\cdot}MeOH$. These are significantly shorter than the Mn–N(amine) lengths—2.034 (3), 2.041 (3) Å in $MnL^2{\cdot}4H_2O$ and 2.073 (4), 2.095 (3) Å in $MnL^3{\cdot}MeOH$. Shorter Mn–N(amide) distances than those observed here have been reported in $Mn^V(O)$–amide species (1.872 (5),[18] 1.888 (5) Å[19]). Among structurally characterized mononuclear manganese(IV) complexes incorporating phenolato coordination, the Mn–O(phenolic) distances lie in the range 1.82–1.92 Å.[2-5] The distances in $MnL^2{\cdot}4H_2O$ and $MnL^3{\cdot}MeOH$ lie close to the lower end of this range.

Both lattices are hydrogen bonded. In $MnL^2{\cdot}4H_2O$ the four water molecules along with the amide oxygen and amine functions constitute a network. The ranges of O---O and O---N distances are 2.796 (6)–2.884 (4) Å and 2.801 (3)–2.872 (5) Å, respectively. In $MnL^3{\cdot}MeOH$, hydrogen bonding is less extensive—each MeOH molecule acting as an intermolecular bridge between an amide oxygen and an amine function (symmetry equivalents of O_3 and N_3; O---O and O---N distances are 2.706 (4) and 2.865 (4) Å, respectively).

EPR Spectra: Small Axial Distortion. The complexes have magnetic moments (Table III) corresponding to the $3d^3$ configuration of manganese(IV). The X-band EPR spectra of the chelates were examined in the polycrystalline phase (300 and 77 K) as well as in 1:1 methanol–toluene glass (77 K). Representative spectra are shown in Figure 4, and relevant parameters are listed in Table III. The spectra of the two complexes are similar. In the polycrystalline phase two broad resonances are observed: a strong one near $g = 2$ and a weak one near $g = 4$. In the magnetically dilute glassy state the ^{55}Mn hyperfine structure is well resolved for the resonance near $g = 2$.

Depending on the nature and extent of distortion of the ligand field from O_h symmetry, the frozen-solution EPR spectra of a $3d^3$ ion can assume different forms.[1,20,21] The form observed here

(18) Collins, T. J.; Gordon-Wylie, S. W. *J. Am. Chem. Soc.* **1989**, *111*, 4511–4513.

(19) Collins, T. J.; Powell, R. D.; Slebodnick, C.; Uffelman, E. S. *J. Am. Chem. Soc.* **1990**, *112*, 899–901.

(strong $g \sim 2$ and weak $g \sim 4$ resonances) is characteristic of small axial distortion: $2D \ll h\nu$, where D is the axial zero-field-splitting parameter and $h\nu$ is the microwave quantum (0.31 cm^{-1} at X-band). When D is small, rhombic splitting is necessarily very small, since $D/E \geq 3$, where E is the rhombic splitting parameter.[20] The value of D has been estimated (Table III) as follows. Between every adjacent pair of the six hyperfine lines of the $g \sim 2$ resonance there is a pair of relatively weak "forbidden" ($\Delta M_S = \pm 1$, $\Delta M_I = \pm 1$) transitions (inset in Figure 4). The magnitude of D can be computed from the intensities of forbidden lines relative to those of allowed lines.[22-24] Within experimental error, both the complexes are found to have the same D value, ~ 125 G or ~ 0.012 cm^{-1}. Whereas the large distortion case $2D \gg h\nu$ occurs in a number of complexes,[2,3,5,6,16,25,26] the $2D \ll h\nu$ situation for manganese(IV) has so far been documented only in tris(dithiocarbamates)[24] ($D \sim 0.013$ cm^{-1}) and in tris(thiohydroxamates)[1] (D not determined) and now in $MnL^2 \cdot 4H_2O$ and $MnL^3 \cdot MeOH$. Interestingly, the ^{55}Mn hyperfine coupling constant for the $g \sim 2$ signal lies close to 95 G for the known $2D \ll h\nu$ manganese(IV) species.

The formal symmetry of the MnN_4O_2 coordination sphere in either complex is only C_1. The EPR results reveal that the amide–amine–phenolate ligand combination provides an effective electronic environment for the metal that is only slightly distorted in the ground state. Further, the distortion is not particularly sensitive to relative geometrical orientation of the donor atoms. The interchange of amide and phenolate positions—as happens between $MnL^2 \cdot 4H_2O$ and $MnL^3 \cdot MeOH$—affects the ground-state distortion only slightly.

Electrochemistry: Low Reduction Potentials. The redox behaviors of the complexes were electrochemically examined at a platinum working electrode, and reduction potential data referenced to a saturated calomel electrode (SCE) are listed in Table I. A well-defined quasireversible one-electron cyclic response is observed near 0.0 V. $E_{1/2}$ of $MnL^2 \cdot 4H_2O$ is slightly more positive than that of $MnL^3 \cdot MeOH$. Exhaustive constant-potential coulometry at −0.30 V consumes one electron and affords a light brown solution whose voltammogram (initial scan anodic) is the same as that of the parent complex (initial scan cathodic). Upon reoxidation at +0.20 V the parent complex is quantitatively regenerated. Thus, the electrode reaction near 0.0 V corresponds to the couple of eq 1. The electrogenerated $[MnL^x]^-$ solution

$$[Mn^{IV}L^x] + e \rightleftharpoons [Mn^{III}L^x]^- \quad (1)$$

is EPR-inactive in the glassy state (77 K), as expected for the d^4 complex. Isolation of $[MnL^x]^-$ as pure salts has eluded us so far. Due to the low reduction potential of the couple of eq 1, MnL^x is rapidly regenerated upon exposure of the electrogenerated $[MnL^x]^-$ solution to air. In the synthesis of MnL^x from H_4L^x and $Mn(CH_3CO_2)_3 \cdot 2H_2O$ it is aerial oxygen that acts as the oxidizing agent.

In a group of manganese(IV) complexes of type MnN_2O_4 the $E_{1/2}$ values have been found to decrease as the pK's of O-donor sites increase (N-donor is invariably imine).[2,3,5a] When N-donors are varied, a similar pK dependence of $E_{1/2}$ for the N-donor sites may be anticipated. On this count MnL^x reduction potentials are indeed expected to be low, since pK's of the amide and amine functions are high (~ 15 and ~ 11, respectively).[27] This has implications for manganese binding in photosystem II, where the metal is known to be coordinated by N and/or O sites, probably more of the latter.[8-10] For water oxidation a high metal reduction potential is necessary. Whereas amide and amine groups are possible biological N-donors, the requirement of high reduction potential would tend to eliminate significant participation of these groups on photosystem II manganese binding.

Concluding Remarks

The main results of this research will now be summarized. Two hexadentate ligands H_4L^x (**1**) incorporating amide, amine, and phenolato functions have been synthesized and employed for binding manganese(IV). The complexes, $MnL^2 \cdot 4H_2O$ and $MnL^3 \cdot MeOH$, have the hitherto unreported nonporphyrinic MnN_4O_2 coordination spheres. The amide nitrogen pairs are coordinated trans to each other in $Mn^{IV}L^2 \cdot 4H_2O$, whereas the phenolic oxygens are trans in $Mn^{IV}L^3 \cdot MeOH$. The coordinated amide groups are approximately planar. The complexes represent the first examples of structurally characterized manganese(IV)–amide and manganese(IV)–amine(aliphatic) binding.

The d^3 complexes display axial X-band EPR spectra with strong and weak signals at $g \sim 2$ and $g \sim 4$. From the intensity of forbidden lines, the axial splitting parameter D is computed to be ~ 0.012 cm^{-1}. We have here the uncommon $2D \ll h\nu$ situation ($h\nu = 0.31$ cm^{-1}). The amide–amine–phenolato ligand combination provides an effective ground-state electronic environment for the metal that is only slightly distorted.

The reduction potential of the manganese(IV)–manganese(III) couple is low, ~ 0.0 V vs SCE. Indeed the trivalent complex is oxidized by air to the tetravalent state. The low metal reduction potentials are in line with the high pK values of the amide and amine functions. These functions are unlikely to be utilized in any major way for manganese binding in photosystem II.

Experimental Section

Materials. $Mn(CH_3CO_2)_3 \cdot 2H_2O$ was prepared as reported.[28] Electrochemically pure CH_3OH and tetraethylammonium perchlorate (TEAP) were obtained as before.[29] All other chemicals and solvents were of analytical grade and used as obtained.

Physical Measurements. Electronic spectra were recorded with a Hitachi 330 spectrophotometer. Magnetic susceptibilities were measured by using a PAR-155 vibrating-sample magnetometer fitted with a Walker Scientific L75FBAL magnet. A Perkin-Elmer 240C elemental analyzer was used to collect microanalytical data (C, H, N). Electrochemical measurements were performed at 298 K under pure and dry nitrogen with a PAR Model 370-4 electrochemistry system as described elsewhere.[2] EPR spectra were measured in the X-band using a Varian 109C spectrometer fitted with a quartz dewar. Calibration was done with DPPH ($g = 2.0037$). The value of the axial parameter D was calculated from the relative intensities of forbidden and allowed lines in the low-field half of the $g \sim 2$ region (frozen solution) according to a reported procedure.[24]

Preparation of Compounds. Ligands. The two ligands, 1,8-bis(2-hydroxybenzamido)-3,6-diazaoctane (H_4L^2) and 1,10-bis(2-hydroxybenzamido)-4,7-diazadecane (H_4L^3), were synthesized using very similar procedures, and details are given for H_4L^2. Ethyl salicylate (13.40 g, 0.08 mol) and triethylenetetramine (5.90 g, 0.04 mol) were taken in a 250-mL beaker, and the mixture was heated on a water bath for 12 h. The mass was then crystallized from a 1:1 ethanol–water mixture, affording a white solid (mp 65–66 °C). The yield was 13.60 g (87%). Anal. Calcd for $C_{20}H_{26}N_4O_4$: C, 62.19; H, 6.73; N, 14.50. Found: C, 62.10; H, 6.68; N, 14.46.

The ligand H_4L^3 was similarly prepared in 97% yield from methyl salicylate and 1,10-diamino-4,7-diazadecane. It was isolated as a colorless semisolid mass. Anal. Calcd for $C_{22}H_{30}N_4O_4$: C, 63.79; H, 7.24; N, 13.52. Found: C, 63.68; H, 7.28; N, 13.42.

Complexes. The two complexes were prepared by the same general procedure, and details are given for $MnL^2 \cdot 4H_2O$. To a 25-mL aqueous methanolic solution of H_4L^2 (1.2 g, 3.10 mmol) was added $Mn(CH_3CO_2)_3 \cdot 2H_2O$ (0.85 g, 3.17 mmol), and the mixture was stirred at room temperature for 1 h. Upon slow evaporation dark colored crystals of $MnL^2 \cdot 4H_2O$ deposited; yield 1.35 g (83%). Anal. Calcd for $MnC_{20}H_{30}N_4O_8$: Mn, 10.79; C, 47.17; H, 5.89; N, 10.99. Found: Mn, 10.82; C, 47.12; H, 5.85; N, 10.96.

(20) Hempel, J. C.; Morgan, L. O.; Lewis, W. B. *Inorg. Chem.* **1970**, *9*, 2064–2072.
(21) Pedersen, E.; Toftlund, H. *Inorg. Chem.* **1974**, *13*, 1603–1612.
(22) Bleaney, B.; Rubins, R. S. *Proc. Phys. Soc. (London)* **1961**, *77*, 103.
(23) Golding, R. M.; Newman, R. H.; Rae, A. D.; Tennant, W. C. *J. Chem. Phys.* **1972**, *57*, 1912–1918.
(24) Brown, K. L.; Golding, R. M.; Healy, P. C.; Jessop, K. J.; Tennant, W. C. *Aust. J. Chem.* **1974**, *27*, 2075–2081.
(25) Richens, D. T.; Sawyer, D. T. *J. Am. Chem. Soc.* **1979**, *101*, 3681–3683.
(26) Lynch, M. W.; Hendrickson, D. N.; Fitzgerald, B. J.; Pierpont, C. G. *J. Am. Chem. Soc.* **1984**, *106*, 2041–2049.
(27) Perrin, D. D.; Dempsey, B.; Serjeant, E. P. *pK_a Prediction for Organic Acids and Bases*; Chapman and Hall: London and New York, 1981.
(28) Brauer, G., Ed. *Handbook of Preparative Inorganic Chemistry*; Academic Press: New York, 1965; Vol. 2, pp 1469–1470.
(29) Datta, D.; Mascharak, P. K.; Chakravorty, A. *Inorg. Chem.* **1981**, *20*, 1673–1679.

Table IV. Crystallographic Data for $MnL^2 \cdot 4H_2O$ and $MnL^3 \cdot MeOH$

	$MnL^2 \cdot 4H_2O$	$MnL^3 \cdot MeOH$
chem formula	$C_{20}H_{30}N_4O_8Mn$	$C_{23}H_{30}N_4O_5Mn$
fw	509.13	497.16
space group	$P2_1/n$ (No. 14)	$P2_1/n$ (No. 14)
a, Å	8.778 (3)	10.369 (4)
b, Å	21.559 (8)	13.639 (8)
c, Å	11.882 (3)	15.753 (7)
β, deg	99.40 (2)	95.61 (3)
V, Å^3	2218 (1)	2217 (2)
Z	4	4
T, °C	23	23
λ, Å	0.71073	0.71073
ρ_{calcd}, g cm^{-3}	1.525	1.490
μ, cm^{-1}	6.23	6.13
transm coeff	0.8756–0.9345	0.8832–0.9418
R,[a] %	4.57	4.58
R_w,[b] %	4.54	4.69
GOF[c]	0.92	1.16

[a] $R = \sum||F_o| - |F_c||/\sum|F_o|$. [b] $R_w = [\sum w(|F_o| - |F_c|)^2/\sum w|F_o|^2]^{1/2}$; $w^{-1} = \sigma^2(|F_o| + g|F_o|^2)$; $g = 0.000\,01$ for $MnL^2 \cdot 4H_2O$ and 0.000 05 for $MnL^3 \cdot MeOH$. [c] The goodness of fit is defined as $[w(|F_o| - |F_c|)^2/(n_o - n_v)]^{1/2}$, where n_o and n_v denote the numbers of data and variables, respectively.

Table V. Atomic Coordinates (×10^4) and Equivalent Isotropic Displacement Coefficients (Å^2 × 10^3) for $MnL^2 \cdot 4H_2O$[a]

atom	x	y	z	U(eq)
Mn	1941 (1)	1663 (1)	4794 (1)	23 (1)
O(1)	2162 (3)	1055 (1)	3747 (2)	31 (1)
O(2)	−2158 (3)	1901 (1)	2591 (2)	38 (1)
O(3)	6052 (3)	1325 (1)	6938 (2)	43 (1)
O(4)	3273 (3)	2203 (1)	4219 (2)	31 (1)
O(1W)	7555 (3)	844 (2)	5137 (3)	56 (1)
O(2W)	5385 (4)	1176 (2)	3161 (3)	67 (1)
O(3W)	5996 (5)	717 (2)	9060 (3)	82 (2)
O(4W)	4326 (5)	574 (2)	936 (3)	80 (2)
N(1)	58 (3)	1970 (1)	3853 (2)	28 (1)
N(2)	1348 (3)	2328 (1)	5857 (2)	28 (1)
N(3)	807 (3)	1080 (1)	5729 (2)	30 (1)
N(4)	3657 (3)	1325 (1)	5876 (2)	30 (1)
C(1)	1050 (4)	794 (2)	2983 (3)	27 (1)
C(2)	1446 (4)	239 (2)	2484 (3)	34 (1)
C(3)	413 (5)	−45 (2)	1633 (3)	39 (1)
C(4)	−1043 (5)	208 (2)	1298 (3)	42 (1)
C(5)	−1439 (4)	749 (2)	1789 (3)	36 (1)
C(6)	−417 (4)	1056 (2)	2638 (3)	28 (1)
C(7)	−885 (4)	1669 (2)	3038 (3)	28 (1)
C(8)	−481 (5)	2586 (2)	4155 (3)	36 (1)
C(9)	676 (5)	2849 (2)	5118 (3)	35 (1)
C(10)	216 (5)	2062 (2)	6536 (3)	37 (1)
C(11)	650 (5)	1395 (2)	6818 (3)	37 (1)
C(12)	1750 (5)	504 (2)	5913 (3)	36 (1)
C(13)	3421 (5)	690 (2)	6276 (4)	44 (1)
C(14)	5013 (4)	1597 (2)	6265 (3)	30 (1)
C(15)	5280 (4)	2235 (2)	5875 (3)	27 (1)
C(16)	6486 (4)	2579 (2)	6492 (3)	34 (1)
C(17)	6852 (4)	3163 (2)	6157 (3)	38 (1)
C(18)	6006 (4)	3424 (2)	5178 (3)	40 (1)
C(19)	4789 (4)	3102 (2)	4562 (3)	35 (1)
C(20)	4426 (4)	2504 (2)	4890 (3)	28 (1)

[a] Equivalent isotropic U defined as one-third of the trace of the orthogonalized U_{ij} tensor.

The complex $MnL^3 \cdot MeOH$ was similarly prepared (yield 86%) by replacing H_4L^2 by H_4L^3 in the above preparation. In spite of the fact that the crystallization medium was the same (aqueous methanol) as above, here only the methanol adduct deposited and no hydrate formation was observed. Anal. Calcd for $MnC_{23}H_{30}N_4O_5$: Mn, 11.05; C, 55.56; H, 6.03; N, 11.26. Found: Mn, 10.95; C, 55.48; H, 6.01; N, 11.29.

X-ray Structure Determination. Unless otherwise indicated the same description applies to both complexes. Cell parameters of the crystals of $MnL^2 \cdot 4H_2O$ (0.14 × 0.16 × 0.40 mm^3) and $MnL^3 \cdot MeOH$ (0.20 × 0.22 × 0.34 mm^3) grown by slow evaporation of aqueous methanolic solutions were determined by least-squares fit of 25 machine-centered reflections (2θ, 15–30°). Lattice dimensions and Laue groups were checked by axial photography. Systematic absences led to space group identification, $P2_1/n$. Data were collected by the ω-scan method (2θ, 2–55°) on a Nicolet R3m/V diffractometer with graphite-monochromated Mo Kα radiation (λ = 0.710 73 Å). Two check reflections measured after every 98 reflections showed no significant intensity reduction during the ~56-h exposure to X-rays. Data were corrected for Lorentz–polarization effects, and an expirical absorption correction was done on the basis of azimuthal scans of six reflections.[30] Of the 5611 ($MnL^2 \cdot 4H_2O$) and 5615 ($MnL^3 \cdot MeOH$) reflections collected, 5084 ($MnL^2 \cdot 4H_2O$) and 5048 ($MnL^3 \cdot MeOH$) were unique of which 3218 ($MnL^2 \cdot 4H_2O$) and 2867 ($MnL^3 \cdot MeOH$) satisfying $I > 3\sigma(I)$ were used for structure solution.

Table VI. Atomic Coordinates (×10^4) and Equivalent Isotropic Displacement Coefficients (Å^2 × 10^3) for $MnL^3 \cdot MeOH$[a]

atom	x	y	z	U(eq)
Mn	1397 (1)	2066 (1)	3863 (1)	27 (1)
O(1)	−249 (2)	1673 (2)	3420 (2)	34 (1)
O(2)	1427 (3)	−908 (2)	4131 (2)	55 (1)
O(3)	3612 (3)	1649 (3)	1932 (2)	50 (1)
O(4)	2926 (2)	2625 (2)	4354 (2)	32 (1)
O(5)	2896 (4)	192 (3)	819 (3)	67 (1)
N(1)	1888 (3)	721 (2)	4148 (2)	32 (1)
N(2)	727 (3)	2166 (3)	5073 (2)	36 (1)
N(3)	627 (3)	3465 (2)	3718 (2)	38 (1)
N(4)	2066 (3)	2139 (2)	2769 (2)	32 (1)
C(1)	−434 (4)	882 (3)	2920 (2)	34 (1)
C(2)	−1443 (4)	911 (3)	2261 (3)	43 (1)
C(3)	−1692 (4)	96 (4)	1764 (3)	49 (1)
C(4)	−963 (5)	−752 (4)	1898 (3)	54 (2)
C(5)	3 (4)	−774 (3)	2543 (3)	45 (1)
C(6)	292 (4)	36 (3)	3059 (3)	38 (1)
C(7)	1270 (4)	−72 (3)	3822 (3)	36 (1)
C(8)	2723 (4)	557 (3)	4949 (2)	38 (1)
C(9)	1991 (5)	762 (3)	5717 (3)	48 (1)
C(10)	1637 (5)	1821 (3)	5803 (3)	49 (2)
C(11)	353 (4)	3196 (3)	5198 (3)	47 (1)
C(12)	−285 (4)	3590 (3)	4374 (3)	46 (1)
C(13)	11 (5)	3740 (3)	2860 (3)	51 (2)
C(14)	915 (5)	3584 (3)	2171 (3)	53 (2)
C(15)	1256 (4)	2526 (3)	2027 (2)	43 (1)
C(16)	3274 (4)	1857 (3)	2650 (2)	34 (1)
C(17)	4274 (3)	1870 (3)	3384 (2)	32 (1)
C(18)	5527 (4)	1547 (3)	3272 (3)	41 (1)
C(19)	6544 (4)	1665 (3)	3883 (3)	44 (1)
C(20)	6339 (4)	2133 (3)	4648 (2)	41 (1)
C(21)	5136 (4)	2455 (3)	4775 (2)	35 (1)
C(22)	4078 (3)	2327 (2)	4163 (2)	29 (1)
C(23)	1566 (6)	157 (4)	642 (4)	69 (2)

[a] Equivalent isotropic U defined as one-third of the trace of the orthogonalized U_{ij} tensor.

The metal atom was located from Patterson maps, and the other non-hydrogen atoms emerged from difference Fourier maps. All non-hydrogen atoms were made anisotropic, and hydrogen atoms were added at calculated position with fixed $U = 0.08$ Å^2 in the last cycle of refinement. All refinements were performed by full matrix least-squares procedures. The number of parameters refined were 298 for each of the two complexes. The highest residuals were 0.36 e/Å^3 ($MnL^2 \cdot 4H_2O$) and 0.59 e/Å^3 ($MnL^3 \cdot MeOH$). All calculations were done on a MicroVAX II computer with the programs of SHELXTL-PLUS.[31] Significant crystal data are listed in Table IV. Atomic coordinates and isotropic thermal parameters are collected in Tables V ($MnL^2 \cdot 4H_2O$) and VI ($MnL^3 \cdot MeOH$).

Acknowledgment. Crystallography was performed at the National Single Crystal Diffractometer Facility at the Department of Inorganic Chemistry, Indian Association for the Cultivation of Science. We are thankful to the Department of Science and Technology, New Delhi, for financial support. Affiliation with the Jawaharlal Nehru Centre for Advanced Scientific Research, Bangalore, India, is acknowledged.

Registry No. H_4L^2, 138606-10-7; H_4L^3, 138606-11-8; $MnL^2 \cdot 4H_2O$, 138606-12-9; $MnL^3 \cdot MeOH$, 138629-02-4; ethyl salicylate, 118-61-6;

(30) North, A. C. T.; Phillips, D. C.; Mathews, F. S. *Acta Crystallogr., Sect. A* **1968**, *24*, 351–359.
(31) Sheldrick, G. M. *SHELXTL*-PLUS *88*, *Structure Determination Software Programs*; Nicolet Instrument Corp.: 5225-2 Verona Road, Madison, WI 53711, 1988.

triethylenetetramine, 112-24-3; methyl salicylate, 119-36-8; 1,10-diamino-4,7-diazadecane, 10563-26-5.

Supplementary Material Available: Listings of anisotropic thermal parameters (Tables VII and VIII), complete bond distances (Tables IX and X) and angles (Tables XI and XII), and hydrogen atom positional parameters (Tables XIII and XIV) for $MnL^2 \cdot 4H_2O$ and $MnL^3 \cdot MeOH$ (7 pages); listings of observed and calculated structure factors for the above two complexes (23 pages). Ordering information is given on any current masthead page.

Contribution from the Dipartimento di Chimica Generale, Università di Pavia, 27100 Pavia, Italy

Using Platinum(II) as a Building Block to Two-Electron Redox Systems. Crystal Structure and Redox Behavior of *cis*-[Pt^{II}(3-ferrocenylpyridine)$_2Cl_2$]

Oliviero Carugo, Giancarlo De Santis, Luigi Fabbrizzi,* Maurizio Licchelli, Alberto Monichino, and Piersandro Pallavicini

Received June 13, 1991

Reaction of 3-ferrocenylpyridine (3-FcPy) with $[Pt^{II}Cl_4]^{2-}$ gave the square complex *cis*-[Pt^{II}(3-FcPy)$_2Cl_2$], which was structurally characterized by X-ray crystallography. The compound, $C_{33}H_{32}Cl_2Fe_2N_2OPt$, containing a disordered acetone molecule, crystallizes in the triclinic $P\bar{1}$ space group, with unit cell parameters a = 9.976 (9) Å, b = 10.53 (1) Å, c = 16.89 (1) Å, α = 106.5 (1)°, β = 97.8 (1)°, γ = 102.8 (1)°, V = 1621 (6) Å^3, Z = 2, and d(calcd) = 1.742 g cm^{-3}. The structure converged to an R factor of 3.5%. *cis*-[Pt^{II}(3-FcPy)$_2Cl_2$], in acetone, DMSO, or MeCN solution, undergoes a two-electron oxidation process, according to two one-electron reversible steps, which involve the two appended ferrocenyl fragments, whose potentials are separated by only the statistical term (36 mV). It is demonstrated that the *cis*-[py_2Pt^{II}] core is a convenient bridging unit to build up novel bis(ferrocene) systems, in which the two relatively close Fc fragments display independent redox activity.

Introduction

Ferrocene is one of the most classical redox agents of organometallic chemistry. Its tendency to undergo a one-electron oxidation process to give the stable ferrocenium ion was demonstrated since its very first appearance on the chemical stage.[1] The ferrocene/ferrocenium (Fc/Fc^+) redox change is so clean and reversible from an electrochemical point of view that ferrocene is more and more frequently used as an internal standard for voltammetric investigations in nonaqueous and poorly polar solvents: ferrocene is dissolved in solution in the same concentration as the investigated electroactive species, and the potential scale is calibrated versus the reversible wave associated with the oxidation of ferrocene. Thus, the Fc^+/Fc couple is now being widely accepted as the nonaqueous counterpart of SHE (or SCE).[2]

Moreover, the ferrocene subunit has been used as a fragment for the design of multielectron redox systems. In particular, bridging two ferrocene subunits generates a redox agent able to exchange a couple of electrons according to two reversible one-electron steps. The mode of the two-electron release by the Fc–R–Fc system (the electron may be exchanged (i) at the same potential or (ii) through two distinct and well-defined steps) depends upon the nature of the bridging fragment R. Bridging of ferrocenyl fragments has been classically carried out by means of carbon chains of varying length and nature: the linking segment may or may not allow communication between the ferrocenyl subunits, influencing the mode of the two-electron release.[3] More recently, Wrighton synthesized 4-ferrocenylpyridine (**1**, 4-FcPy),

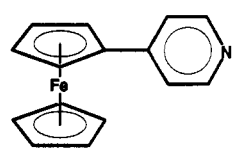

1

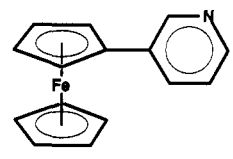

2

which has been designed as a ligand containing a pendant redox active unit. Reaction of 4-FcPy with $Re(CO)_5Cl$ gave the Re-(4-FcPy)$_2$(CO)$_3$Cl complex.[4] This species has an octahedral stereochemistry, and the two 4-FcPy molecules occupy adjacent coordination sites, as indicated by the identical NMR parameters of the two pyridine ligands. *fac*-(4-FcPy)$_2$(CO)$_3$Cl, which was designed with the aim to modulate the spectroscopic properties of the metal center (Re) by changing the oxidation state of the peripheral Fc subunits, represents a novel example of bis(ferrocene), in which the bridging unit is a transition-metal coordination compound: e.g. the *cis*-Py_2Re^+ core. It should be noted that using bridging segments derived from organic chemistry gives angles of 109, 120, and 180°, according to the type of hybridization of the carbon atom(s). The novelty of using transition-metal centers as bridging segments is that the envisaged redox units (e.g. Fc) can be situated at different angles.

We wished to further explore this possibility by binding two ferrocenylpyridine molecules to a transition-metal center prone to a cis type of coordination. In particular, we used 3-ferrocenylpyridine (**2**, 3-FcPy), which can be conveniently obtained through a *one-pot* synthesis, which involves diazo coupling of ferrocene and pyridine. Reaction of 3-FcPy with $[Pt^{II}Cl_4]^{2-}$ gave the *cis*-[Pt^{II}(3-FcPy)$_2Cl_2$] complex. Pt^{II} was chosen as a metal center as it gives with ligands containing nitrogen donor atoms complexes which are very stable from both a thermodynamic and a kinetic point of view. Due to its preferred cis mode of coordination, Pt^{II} as a bridging segment should be able to place the two ferrocene subunits along two planes which form an angle different from those generally obtained by using segments derived from organic chemistry. This work describes the crystal and molecular structure of *cis*-[Pt^{II}(3-FcPy)$_2Cl_2$] as well as its solution behavior, with a special regard to the two-electron oxidation process to give *cis*-[Pt^{II}(3-FcPy$^+$)$_2Cl_2$]$^{2+}$.

Experimental Section

Ferrocene (Fluka) was recrystallized from hexane. All other reagents and starting materials used in the synthetic work were used as received. ^{1}H NMR spectra (solvent $CDCl_3$, internal TMS standard) were measured on 80- or 300-MHz Bruker instruments. UV–vis spectra were recorded on a Hewlett-Packard 8452 diode-array spectrometer.

3-Ferrocenylpyridine (3-FcPy) (2). Synthesis of the ligand was performed by using a modification of the literature method.[5] 3-Aminopyridine (0.1 mol) was dissolved in aqueous 20% HCl (100 mL). To this

(1) Wilkinson, G.; Rosenblum, M.; Whiting, M. C.; Woodward, R. D. *J. Am. Chem. Soc.* **1952**, *74*, 2125.
(2) Gritzner, G.; Küta, J. *Pure Appl. Chem.* **1984**, *56*, 462 and references therein.
(3) Morrison, W. H., Jr.; Krogsrud, S.; Hendrickson, D. N. *Inorg. Chem.* **1973**, *12*, 1998.
(4) Miller, T. M.; Kazi, J. A.; Wrighton, M. S. *Inorg. Chem.* **1989**, *28*, 2347.
(5) Schlögl, K.; Fried, M. *Monatsh. Chem.* **1963**, *94*, 537.

0020-1669/92/1331-0765$03.00/0